Stress concentration during pellet cladding interaction: Comparison of closed-form solutions with 2D(r,θ) finite element simulations

Jérôme Sercombe, Renaud Masson, Thomas Helfer

Article publié dans
Nuclear Engineering and Design, 2013, vol. 260, p. 175-187.

Stress concentration during pellet cladding interaction: Comparison of closed-form solutions with 2D(r,θ) finite element simulations

Jérôme Sercombe[a,*], Renaud Masson[b,1], Thomas Helfer[a]

[a] CEA, DEN, DEC/SESC, F-13108 Saint-Paul-lez-Durance, France
[b] CEA DEN, F-13108 Saint-Paul-Lez-Durance, France

HIGHLIGHTS

- This paper presents closed-formed solutions concerning pellet cladding interaction.
- First, the opening of a radial crack in a pellet fragment is estimated.
- Second, the stresses in the cladding in front of the pellet crack are calculated.
- The closed-formed solutions are found in good agreement with 2D FE simulations.
- They are then used in the fuel code ALCYONE to model PCI during power ramps.

ARTICLE INFO

Article history:
Received 29 May 2012
Received in revised form 12 March 2013
Accepted 13 March 2013

ABSTRACT

This paper presents two closed-form solutions that can be used to enrich the mechanical description of fuel pellets and cladding behavior in standard one-dimensional based fuel performance codes. The first one is concerned with the estimation of the opening of a radial crack in a pellet fragment induced by the radial thermal gradient in the pellet and limited by the pellet-clad contact pressure. The second one describes the stress distribution in a cladding bore in front of an opening pellet crack. A linear angular variation of the pellet-clad contact pressure and a constant prescribed radial displacement are considered. The closed-form solutions are checked by comparison to independent finite element models of the pellet fragment and of the cladding. Their ability to describe non-axisymmetric displacement and stress fields during loading histories representative of base irradiation and power ramps is then demonstrated by cross-comparison with the 2D pellet fragment-cladding model of the multi-dimensional fuel performance code ALCYONE. The calculated radial crack opening profiles at different times and the hoop stress concentration in the cladding at the top of the ramp are found in good agreement with ALCYONE.

1. Introduction

Failure of zirconium alloys fuel rods by pellet cladding interaction (PCI) has been studied worldwide for many years (Cox, 1990) but remains a matter of concern since no absolute remedy has yet been found. On a mechanical standpoint, the main parameters that govern PCI failures are however well known: pellet hourglassing or wheatsheaf due to the high radial thermal gradient in the pellet which leads to over-straining of the cladding in front of pellet ends (Levy and Wilkinson, 1974), pellet radial cracking which induces strain-stress concentration in the cladding (Gittus, 1972) and friction at the pellet-cladding interface which maximize interfacial shear and circumferential stresses in the cladding (Ranjan and Smith, 1980).

Fuel performance codes are generally based on a radial one-dimensional description of the fuel pellet and the cladding (Lassmann, 1988) and hence cannot provide estimates of stress or strain concentration in front of an opening radial pellet crack which is by essence a two-dimensional problem. Some authors have derived closed-form solutions to estimate the stress concentration factor in function of the applied thermal and mechanical loadings on the pellet and the cladding (Gittus, 1972; Roberts, 1978; Ranjan and Smith, 1980; Nakatsuka, 1981; Jackson, 1987; Retel et al., 2004). A first mechanical description based on membrane shell theory (constant hoop stress across the cladding wall) was proposed by Gittus (1972) for the estimation of strain concentration over an opening pellet crack. The hoop strain at the cladding inner surface was found to vary exponentially with angular position

* Corresponding author at: CEA CADARACHE, DEN/DEC/SESC/LSC - Bât. 151, 13108 Saint-Paul-Lez-Durance, France. Tel.: +33 4 42 25 30 72; fax: +33 4 42 25 29 49.
E-mail address: jerome.sercombe@cea.fr (J. Sercombe).
[1] Formerly EDF R&D, Les Renardières, 77250 Moret sur Loing, France.

with a maximum located at the pellet crack tip where shear stresses change sign. By solving the problem of an infinitely thick flat clad submitted on its inner surface to a uniform pressure and uniform shear stresses with periodic change in its direction, Ranjan and Smith (1980) proposed a closed-form solution for stress and strain evolution through the cladding thickness. Based on finite element analyses, this first solution was extended to the more realistic case of a cladding with a prescribed uniform radial displacement on its inner wall, as expected if the fuel is more rigid than the cladding. Roberts (1978) analyzed the problem of a curved cladding of finite thickness using the stress function approach in which the normal and shear stresses at the cladding bore and surface were expanded in terms of Fourier series. The stress and strain distribution along the cladding thickness was thus estimated in the case of a uniform or exponential variation of the contact pressure and shear stresses with angular position. Jackson (1987) extended Roberts' analysis to the case of a linear variation of contact pressure with angular position and a pressure differential acting across the cladding. Nakatsuka (1981) proposed an approximate solution for stress and strain evolution through the clad thickness based on plate bending theory which he compared to PCMI expanding mandrel test measures. Retel et al. (2004) developed a curvilinear thin beam model for the cladding to catch the stress concentration resulting from the discontinuous contact pressure and the pellet radial cracks. Some of these models are used in fuel performance codes to improve the one-dimensional description of PCI (Yaung et al., 1985; Baron et al., 2008). A pre-requisites to stress concentration models is that the crack opening at the crack tip is known. In this respect, so-called hoop enrichment models have recently been developed to trigger the impact of the thermal gradient, of solid swelling and of the contact pressure in a pellet fragment on the crack opening (Baron et al., 2008).

Nowadays, progress in computational performance and finite element codes has made possible the simulation of the thermo-mechanical behavior of a fragmented pellet enclosed in a viscoplastic cladding (Brochard et al., 2001; Marchal et al., 2009). Two- or three-dimensional simulations of this problem are thus proposed in the fuel code ALCYONE (Michel et al., 2008; Sercombe et al., 2009) where the angular (and axial) distribution of the pellet-clad interfacial contact pressure and shear stresses can be estimated at any time of a power transient. Provided the mesh refinement is sufficient, the stress and strain concentration in the cladding in front of the pellet crack can be described, particularly in two-dimensional calculations (Michel et al., 2008). The complexity of the problem is due to the high level of interaction between adjacent pellet fragments (with partial crack closure along the pellet radius) and at the pellet clad interface (unilateral contact and friction). In practice, it is important to assess the validity of the stress and strain states in the cladding resulting from PCI as estimated by the finite element method. In this respect, closed-form solutions can also be useful.

In this paper, closed-form solutions which give the opening of a pellet radial crack and the resulting stress intensification in the cladding during typical in-reactor loading sequences are proposed and compared to two-dimensional simulations of PCI performed with the fuel code ALCYONE.

2. Pellet fragment crack opening model

2.1. Muskhelishvili's formulation

Here, we consider a uniform bi-dimensional solid obeying to an elastic isotropic behavior (G and ν denote the shear modulus and the Poisson's ratio of this body). If no body forces are applied to this solid and considering plane strain conditions, the two components

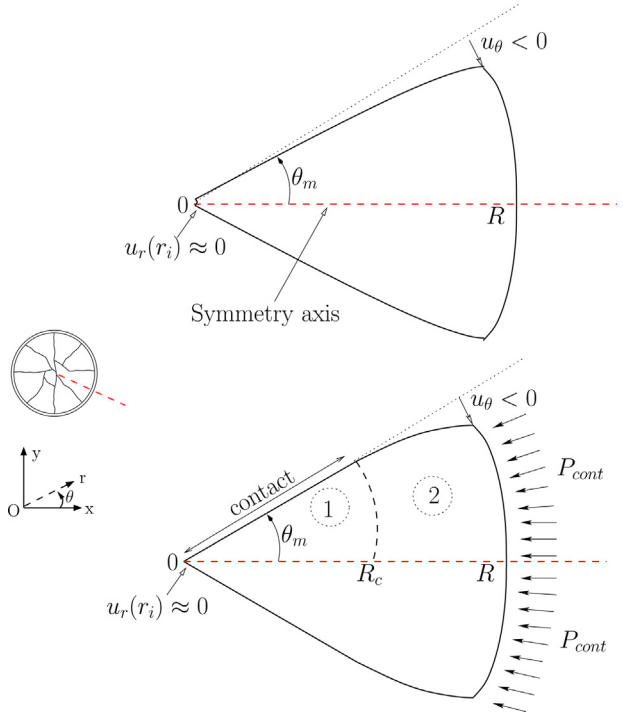

Fig. 1. Pellet fragment submitted to an isotropic swelling only (top), pellet fragment submitted to an isotropic swelling and a contact pressure with two zones delimited by the contact radius (bottom).

of the displacement field, denoted by $u_x(x, y)$ and $u_y(x, y)$ in cartesian coordinates, can be expressed as a function of two potentials $(\Omega(z), w(z))$ of the complex variable $z = x + iy$ as (Muskhelishvili, 1963):

$$u_x + iu_y = D(z) = \frac{1}{2G}\left[(3-4\nu)\Omega(z) - z\overline{\Omega'(z)} - \overline{w(z)}\right] \quad (1)$$

where $\bar{z}$ denotes the conjugate of the complex number z. If this body is submitted to an isotropic stress free strain field $\hat{\epsilon}^{an}(x, y)$, additional terms appear in the former expression. When this stress free strain field $\hat{\epsilon}^{an}$ depends only on the radius $r = \sqrt{z\bar{z}} = \sqrt{x^2 + y^2}$, these additional terms read:

$$D(z) = \frac{1}{2G}[(3-4\nu)\Omega(z) - z\overline{\Omega'(z)} - \overline{w(z)}] + \epsilon_1^{an} z + \epsilon_2^{an}(z\,ln(z) - z) + \frac{1}{2}\left(\frac{1+\nu}{1-\nu}\right)\frac{1}{\bar{z}}\left(\int_0^{\sqrt{z\bar{z}}} 2t\epsilon^{an}(t)dt\right) \quad (2)$$

the stress free strain being decomposed as: $\hat{\epsilon}^{an}(r) = \epsilon_1^{an} + \epsilon_2^{an} r + \epsilon^{an}(r)$. The strain and stress fields can be derived from the displacement field by elementary algebraic manipulations. If the derivatives of the two complex potential are holomorphic functions of the complex variable, the stress field satisfies the equilibrium equations.

2.2. Application to a pellet fragment submitted to an isotropic swelling

The pellet is divided in N identical fragments. In this section, the pellet cladding gap is open (see top Fig. 1). The internal pressure being neglected, the outer surface of the pellet fragments is free. The loading is a stress-free strain radial distribution corresponding to an isotropic swelling approximated by: $\epsilon^{an} = \sum_{k\geq 2} \epsilon_{k+1}^{an} r^k$. In this general expression, the thermal strain gradient corresponds to $k = 2$.

In that situation, the two complex potentials are chosen as follows:

$$\begin{aligned}\Omega(z) &= \sum_{k\geq 3}\alpha_k\epsilon_k^{an}z^k + A\ln\left(\frac{z}{r_0}\right)\\ w(z) &= \sum_{k\geq 3}\beta_k\epsilon_k^{an}z^k - A\ln\left(\frac{z}{r_0}\right)\end{aligned} \tag{3}$$

(α_k, β_k) being necessary real due to symmetry considerations. The displacement field can be easily deduced from Eqs. (3). The radial and tangential components of displacement reads:

$$\begin{aligned}u_r &= \sum_{k\geq 3}\epsilon_k^{an}\left[\frac{1+\nu}{1-\nu}\frac{1}{k+1} + \frac{1}{2G}((3-4\nu-k)\alpha_k\cos((k-1)\theta) - \beta_k\cos((k+1)\theta))\right]r^k + \frac{A}{2G}\left[(4-4\nu)\cos(\theta)\ln\left(\frac{r}{r_0}\right) + (2-4\nu)\theta\sin(\theta) - \cos(\theta)\right]\\ u_\theta &= \frac{1}{2G}\sum_{k\geq 3}\epsilon_k^{an}[(3-4\nu+k)\alpha_k\sin((k-1)\theta) + \beta_k\sin((k+1)\theta)]r^k + \frac{A}{2G}\left[(2-4\nu)\theta\cos(\theta) - (4-4\nu)\sin(\theta)\ln\left(\frac{r}{r_0}\right) - \sin(\theta)\right]\end{aligned} \tag{4}$$

while the stress distribution is given by:

$$\begin{aligned}\sigma_{r\theta} &= \sum_{k\geq 3}k\epsilon_k^{an}r^{k-1}[(k-1)\alpha_k\sin((k-1)\theta) + \beta_k\sin((k+1)\theta)]\\ \sigma_{\theta\theta} &= \sum_{k\geq 3}k\epsilon_k^{an}r^{k-1}\left[-\frac{1+\nu}{1-\nu}\frac{2G}{k+1} + (1+k)\alpha_k\cos((k-1)\theta) + \beta_k\cos((k+1)\theta)\right]\\ \sigma_{rr} &= \sum_{k\geq 3}\epsilon_k^{an}r^{k-1}\left[-\frac{1+\nu}{1-\nu}\frac{2G}{k+1} + k((3-k)\alpha_k\cos((k-1)\theta) - \beta_k\cos((k+1)\theta))\right] + \frac{4A}{r}\cos(\theta).\end{aligned} \tag{5}$$

It's worth noticing that the displacement as well as the stress fields are singular at the apex of the fragment. To avoid these singularities, a small region close to this apex ($0 \leq r \leq r_i$ with r_i/R less than a few percent) is truncated and the parameter r_0 is chosen such that the radial displacement at $r = r_i$ is zero in an average sense, namely:

$$\frac{1}{2\theta_m}\int_{-\theta_m}^{\theta_m} u_r(r_i,\theta)d\theta = 0 \tag{6}$$

or, equivalently:

$$\begin{aligned}&\sum_{k\geq 3}\epsilon_k^{an}r_i^k\left[\frac{1+\nu}{1-\nu}\frac{\theta_m}{k+1} + \frac{1}{2G}\left(\frac{3-4\nu-k}{k-1}\alpha_k\sin((k-1)\theta_m)\right.\right.\\ &\left.\left. - \frac{\beta_k}{k+1}\sin((k+1)\theta_m)\right)\right] + \frac{A}{2G}\left[(4-4\nu)\sin(\theta_m)\ln\left(\frac{r_i}{r_0}\right)\right.\\ &\left. + (2-4\nu)(\sin(\theta_m) - \theta_m\cos(\theta_m)) - \sin(\theta_m)\right] = 0\end{aligned}$$

The unknown constants (α_k, β_k) are calculated with respect to the following boundary conditions:

$$\sigma_{\theta\theta}(r,\pm\theta_m) = \sigma_{r\theta}(r,\pm\theta_m) = 0 \quad for \quad r_i \leq r \leq R. \tag{7}$$

which reflect the lack of contact between neighboring pellet fragments. It yields:

$$\begin{aligned}\alpha_k &= \frac{1+\nu}{1-\nu}\frac{2G}{k+1}\frac{\sin((k+1)\theta_m)}{\sin(2k\theta_m) + k\sin(2\theta_m)}\\ \beta_k &= \frac{1+\nu}{1-\nu}\frac{2G}{k+1}\frac{(1-k)\sin((k-1)\theta_m)}{\sin(2k\theta_m) + k\sin(2\theta_m)}\end{aligned} \tag{8}$$

Finally, its is remarked that the shear and normal components of the stress vector at $r = R$ depend on the angle θ and are non-zero. As a result, the stress field is not rigorously statically admissible. However, the average shear component of the stress vector on the pellet periphery as given by:

$$\frac{1}{2\theta_m}\int_{-\theta_m}^{\theta_m}\sigma_{r\theta}(R,\theta)d\theta \tag{9}$$

vanishes while the constant A is chosen such that the average radial stress on the pellet periphery equals zero, namely:

$$\begin{aligned}A = \frac{1}{4\sin(\theta_m)}\sum_{k\geq 3}\epsilon_k^{an}R^k\left[\frac{2G}{k+1}\frac{1+\nu}{1-\nu}\theta_m\right.\\ \left. + k\left(\alpha_k\frac{k-3}{k-1}\sin((k-1)\theta_m) - \frac{\beta_k}{k+1}\sin((k+1)\theta_m)\right)\right]\end{aligned} \tag{10}$$

2.3. Impact of the contact pressure

When the pellet cladding gap closure is achieved, the pellet fragments are submitted to contradictory effects: the swelling strain gradient tends to open the radial cracks while the contact pressure has an opposite effect. The balance between these two phenomena is represented by a contact radius (denoted as R_c in Fig. 1). To derive relevant approximations of the displacement field, the pellet fragment is modeled as two zones (see Fig. 1). In the first zone ($0 \leq r \leq R_c$), pellet fragments are in contact and the displacement field is given by (axisymmetric solution with $\Omega(z) = \gamma z$ where γ is a constant parameter and $w(z) = 0$):

$$\begin{aligned}u_r &= \frac{\gamma}{G}(1-2\nu)r + \sum_{k\geq 3}\epsilon_k^{an}\frac{1+\nu}{1-\nu}\frac{r^k}{k+1}\\ u_\theta &= 0\end{aligned} \tag{11}$$

In the second zone ($R_c \leq r \leq R$), the two complex potentials are similar to the ones given previously by relation (3). The displacement and stress fields in this zone are still given by relations (4) and (5), respectively (for $R_c \leq r \leq R$). To ensure the condition (7) on $R_c \leq r \leq R$, the coefficients (α_k, β_k) are given by relations (8) while the coefficient A is such that the average radial stress on the pellet periphery equilibrates the contact pressure, namely:

$$\begin{aligned}A = \frac{R}{4\sin(\theta_m)}\left\{-P_c\,\theta_m + \sum_{k\geq 3}\epsilon_k^{an}R^{k-1}\left[\frac{2G}{k+1}\frac{1+\nu}{1-\nu}\theta_m\right.\right.\\ \left.\left. + k\left(\alpha_k\frac{k-3}{k-1}\sin((k-1)\theta_m) + \frac{\beta_k}{k+1}\sin((k+1)\theta_m)\right)\right]\right\}\end{aligned} \tag{12}$$

With this approximated solution, the displacement field cannot be continuous on the boundary between the two zones ($r = R_c$). However, the best approximation is derived by forcing this continuity condition at the particular point (R_c, θ_m), namely:

$$\begin{aligned}u_\theta^{zone2}(R_c,\theta_m) &= 0\\ u_r^{zone1}(R_c,\theta_m) &= u_r^{zone2}(R_c,\theta_m)\end{aligned} \tag{13}$$

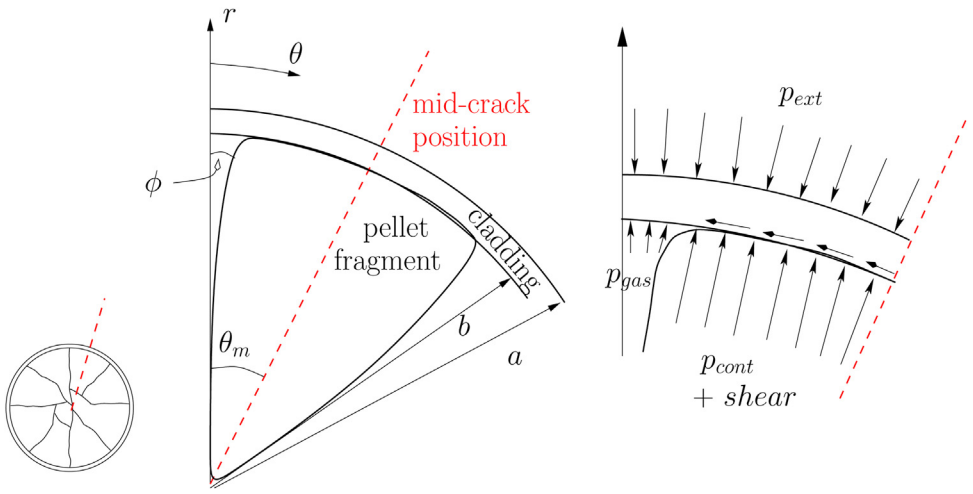

Fig. 2. Schematic fuel clad model used in the calculations.

These additional relations allow to determine the value of the parameter r_0 and of the contact radius R_c:

$$\ln(r_0) = \ln(R_c) - \left(\frac{(2-4\nu)\theta_m\, cos(\theta_m) - sin(\theta_m)}{(4-4\nu)sin(\theta_m)}\right) - \frac{F(R_c)}{(4-4\nu)A\, sin(\theta_m)} \tag{14}$$

$$\gamma(2-4\nu)R_c = \sum_{k\geq 3}\epsilon_k^{an}R_c^k\left[(3-4\nu-k)\alpha_k\cos((k-1)\theta_m) - \beta_k\cos((k+1)\theta_m)\right] + A\left[(4-4\nu)\cos(\theta_m)\ln\left(\frac{R_c}{r_0}\right) + (2-4\nu)\theta_m\sin(\theta_m) - \cos(\theta_m)\right] \tag{15}$$

with

$$F(R_c) = \sum_{k\geq 3}\epsilon_k^{an}R_c^k[(3-4\nu+k)\alpha_k sin((k-1)\theta_m) + \beta_k sin((k+1)\theta_m)] \tag{16}$$

The last closure relation is obtained by ensuring the continuity of the radial stress at the same particular point (R_c, θ_m):

$$\sigma_{rr}^{zone1}(R_c,\theta_m) = \sigma_{rr}^{zone2}(R_c,\theta_m) \tag{17}$$

3. Stress concentration over an opening pellet crack

3.1. Roberts' solution

In its paper, Roberts (1978) studied the case of a pellet divided by N regularly spaced cracks having an angular displacement of $2\theta_m$ between each one and a crack width of 2ϕ, as represented in Fig. 2. The external pressure was assumed equal to zero. A uniform normal pressure on the inner cladding surface was assumed to act together with a shear stress which depends on the normal pressure and frictional coefficient. Thus, the problem resolved into a standard one, namely finding the distribution of elastic stresses in a thick-walled cylinder having specified normal and shear stresses on the inner and outer surfaces. Roberts (1978) showed that an Airy stress function of the following form could satisfy the compatibility equation and the symmetries of the problem:

$$\Phi = A_0 r^2 + B_0 \ln r + \sum_{m=2}^{\infty}(A_m r^{m+2} + B_m r^{-m} + C_m r^m + D_m r^{-m+2}) \times \cos(m\theta) \tag{18}$$

with A_0, B_0, A_m, B_m, C_m and D_m constant parameters. For the proposed stress function, the plane strain stresses are:

$$\begin{aligned}
\sigma_{rr} &= 2A_0 + \frac{B_0}{r^2} - \sum_{m=2}^{\infty}[(m+1)(m-2)A_m r^m + m(m+1)B_m r^{-m-2} + m(m-1)C_m r^{m-2} + (m-1)(m+2)D_m r^{-m}]\cos(m\theta)\\
\sigma_{\theta\theta} &= 2A_0 - \frac{B_0}{r^2} - \sum_{m=2}^{\infty}[(m+1)(m+2)A_m r^m + m(m+1)B_m r^{-m-2} + m(m-1)C_m r^{m-2} + (m-1)(m-2)D_m r^{-m}]\cos(m\theta)\\
\sigma_{r\theta} &= \sum_{m=2}^{\infty}[m(m+1)A_m r^m - m(m+1)B_m r^{-m-2} + m(m-1)C_m r^{m-2} - m(m-1)D_m r^{-m}]\sin(m\theta)
\end{aligned} \tag{19}$$

The displacements are given by:

$$\begin{aligned}
u_r &= \frac{1}{G}\left\{2A_0(1-2\nu)r - \frac{B_0}{r} + \sum_{m=2}^{\infty}[(2(1-2\nu)-m)A_m r^{m+1} + mB_m r^{-m-1} - mC_m r^{m-1} + (2(1-2\nu)-m)D_m r^{-m+1}]\cos(m\theta)\right\}\\
u_\theta &= \frac{1}{G}\left\{\sum_{m=2}^{\infty}[(m+4(1-\nu))A_m r^{m+1} + mB_m r^{-m-1} + mC_m r^{m-1} + (m+4(1-\nu))D_m r^{-m+1}]\sin(m\theta)\right\}
\end{aligned} \tag{20}$$

In the above expressions, σ_{rr} denotes the radial, $\sigma_{\theta\theta}$ the hoop and $\sigma_{r\theta}$ the shear stress. The radial and circumferential displacements are signified by u_r and u_θ, respectively.

3.2. Closed-form solution for a prescribed uniform radial displacement

Here, the original formulation proposed by Roberts has been modified to account for boundary conditions closer to those taking place in a PWR fuel rod: the external pressure of the coolant p_{ext} is assumed non zero, a linear evolution of the contact pressure with angular position $p_{cont} = K_1\theta + K_2$ is assumed. In its paper, Jackson (1987) proposed a similar extension of Roberts analysis to a pressure differential across the cladding and allowing for a linear variation of the fuel-clad contact pressure. In this paper, we consider in addition the fuel rod gas pressure p_{gas}, applied on the part of the inner clad surface which is not in contact with the pellet ($-\phi \le \theta \le \phi$), see Fig. 2. In the present case, the boundary conditions are thus given by:

$$\begin{cases} \sigma_{rr}(a) = p_{ext} & \text{and} \quad \sigma_{r\theta}(a) = 0 & & \\ \sigma_{rr}(b) = p_{gas} & \text{and} \quad \sigma_{r\theta}(b) = 0 & \text{for} \quad -\phi \le \theta \le \phi & \\ \sigma_{rr}(b) = p_{cont}(\theta) & \text{and} \quad \sigma_{r\theta}(b) = \mu\sigma_{rr} & \text{for} \quad \phi \le \theta \le \theta_m & \\ \sigma_{rr}(b) = p_{cont}(\theta) & \text{and} \quad \sigma_{r\theta}(b) = -\mu\sigma_{rr} & \text{for} \quad -\theta_m \le \theta \le -\phi & \end{cases} \tag{21}$$

with μ the constant pellet-clad friction coefficient. The boundary conditions reflect the discontinuity of the contact pressure and shear stresses on the inner surface of the cladding due to the pellet crack opening ($-\phi \le \theta \le \phi$).

Solving the problem requires the determination of the contant parameters A_0, B_0, A_m, B_m, C_m and D_m. The constants A_0 and B_0 relate to the uniform stressing of a thickwalled elastic cylinder and may be obtained directly from the boundary conditions $\sigma_{rr}(a) = p_{ext}$ on the outer surface, and $\sigma_{rr}(b) = p_{cont}^{mean}$ on the inner surface. p_{cont}^{mean} is the average contact pressure applied on the inner surface.

$$\begin{aligned} A_\circ &= \frac{p_{cont}^{mean} b^2 - p_{ext} a^2}{2(b^2 - a^2)} \\ B_\circ &= a^2 b^2 \frac{p_{ext} - p_{cont}^{mean}}{b^2 - a^2} \end{aligned} \tag{22}$$

Use of the boundary conditions on the external clad surface ($\sigma_{rr}(a) = p_{ext}$ and $\sigma_{r\theta}(a) = 0$) in the plain strain stresses given by relations (19) leads the two following equations for the remaining coefficients A_m, B_m, C_m and D_m:

$$\begin{aligned} &(m+1)(m-2)A_m^* + m(m+1)B_m^* + m(m-1)C_m^* \\ &\quad + (m-1)(m+2)D_m^* = 0 \end{aligned} \tag{23}$$

and

$$m(m+1)A_m^* - m(m+1)B_m^* + m(m-1)C_m^* - m(m-1)D_m^* = 0 \tag{24}$$

with

$$A_m^* = A_m a^m; \quad B_m^* = B_m a^{-m-2}; \quad C_m^* = C_m a^{m-2}; \quad D_m^* = D_m a^{-m} \tag{25}$$

To complete the system, a Fourier expansion of the boundary conditions applied on the inner clad surface ($r = b$) is used with the requirement that these expressions are equal to the stresses given by Eqs. (19). Expressing the variation of the circumferential and shear stresses on the inner surface of the cladding as Fourier sums leads $\sigma_{rr}(b)$ and $\sigma_{r\theta}(b)$ in the following form:

$$\begin{aligned} \sigma_{rr}(b) &= p_{cont}^{mean} + \sum_{i\ge1} \left(\frac{2(p_{gas} - K_2)\sin(iN\phi)}{i\pi} - \frac{2K_1}{i^2\pi N}\left[iN\phi\sin(iN\phi) + \cos(iN\phi) - (-1)^i \right] \right) \cos(iN\theta) \\ \sigma_{r\theta}(b) &= 2\mu \sum_{i\ge1} \left(K_2 \frac{\left[\cos(iN\phi) - (-1)^i\right]}{i\pi} + \frac{K_1}{i\pi N}[N\phi\cos(iN\phi) - \pi(-1)^i] - \frac{K_1}{i^2\pi N}\sin(iN\phi) \right) \sin(iN\theta) \end{aligned} \tag{26}$$

Comparison of these expressions with the stresses (see equations (19) with $r = b$) shows that m will be summed multiples of N, i.e., $m = iN$. The remaining two equations for A_m, B_m, C_m and D_m follow from the comparison and are given by:

$$\begin{aligned} &(m+1)(m-2)A_m^* R_s^m + m(m+1)B_m^* R_s^{-m-2} + m(m-1)C_m^* R_s^{m-2} \\ &\quad + (m-1)(m+2)D_m^* R_s^{-m} = -\alpha_m \end{aligned} \tag{27}$$

$$\begin{aligned} &(m+1)(m-2)A_m^* R_s^m - m(m+1)B_m^* R_s^{-m-2} + m(m-1)C_m^* R_s^{m-2} \\ &\quad - m(m-1)D_m^* R_s^{-m} = \beta_m \end{aligned} \tag{28}$$

with

$$\begin{aligned} -\alpha_m &= -\frac{2(p_{gas} - K_2)\sin(m\phi)}{i\pi} + \frac{2K_1}{i^2\pi N}[iN\phi\sin(iN\phi) - ((-1)^i - \cos(iN\phi))] \\ \beta_m &= 2\mu K_2 \frac{(\cos(iN\phi) - (-1)^i)}{i\pi} + \frac{2\mu K_1}{i\pi N}(N\phi\cos(iN\phi) - \pi(-1)^i) - \frac{2\mu K_1}{i^2\pi N}\sin(iN\phi) \end{aligned} \tag{29}$$

and $R_s = b/a$. For each summation index $m = iN$, the system of Eqs. (23), (24), (27) and (28) are sufficient to determine the constants A_m, B_m, C_m and D_m. In the case of the linear evolution of the contact pressure with θ considered here, $p_{cont}(\theta) = K_1\theta + K_2$, the parameters A_m, B_m, C_m and D_m can be expressed in function of K_1 and K_2. To further simplify the system, it may be noticed that for a linear evolution of the contact pressure, K_2 reads as follows in function the slope K_1:

$$K_2 = p_{cont}^{mean} - K_1 \frac{\theta_m + \phi}{2} \tag{30}$$

In turn, this means that it is possible to express the parameters A_m, B_m, C_m and D_m as linear functions of K_1 only.

$$X_{iN} = X_{iNx} + X_{iNy}.K_1 \tag{31}$$

with $X = A^*, B^*, C^*$ or D^*. In Eq. (31), m has been replaced by iN.

Since the clad materials (Zircaloy based alloys) are usually two to three times softer than uranium dioxide, pellet cladding interaction is conveniently described by applying an azimuthally uniform radial displacement on the inner clad surface rather than a constant pressure. This point was discussed by Ranjan and Smith (1980) and led to the derivation of their so-called hard pellet model. Jackson (1987) showed furthermore by finite element analysis that a linear variation in contact pressure can lead to a substantial reduction in the variation of the radial displacement.

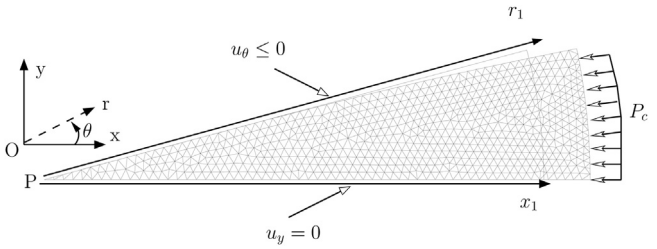

Fig. 3. Deformed pellet fragment mesh and boundary conditions in the finite element simulations with Cast3M ($N = 12$).

If we now use the relations (31) in Eq. (20), it is possible to express the radial displacement at the inner surface of the cladding ($u_r(b, \theta)$) also as a linear function of K_1:

$$u_r(b,\theta) = \frac{A_\circ}{G}(1-2\nu)b - \frac{B_\circ}{2Gb} + \frac{a}{2G}\sum_{i\geq 1}(U_{iNx} + K_1 U_{iNy})\cos(iN\theta) \tag{32}$$

with

$$\begin{cases} U_{iNx} &= [2(1-2\nu) - iN]A^*_{iNx}R_s^{iN+1} + iNB^*_{iNx}R_s^{-iN-1} - iNC^*_{iNx}R_s^{iN-1} + [2(1-2\nu) + iN]D^*_{iNx}R_s^{-iN+1} \\ U_{iNy} &= [2(1-2\nu) - iN]A^*_{iNy}R_s^{iN+1} + iNB^*_{iNy}R_s^{-iN-1} - iNC^*_{iNy}R_s^{iN-1} + [2(1-2\nu) + iN]D^*_{iNy}R_s^{-iN+1} \end{cases} \tag{33}$$

Achieving a constant radial displacement on the inner clad wall is by essence impossible with Roberts' approach. In this work, to fulfill that condition as much as possible, and hence to approach the case of a hard pellet, a minimization of the angular variation of the radial displacement is enforced by adding the following condition on the contact pressure slope:

$$\min_{K_1}\left\{\int_\phi^{\theta_m}[u_r(b,\theta) - u_r(b,\theta_m)]^2 d\theta\right\} \tag{34}$$

which can be expressed as:

$$2\int_\phi^\theta [u_r(b,\theta) - u_r(b,\theta_m)] \times \left[\frac{\partial u_r}{\partial K_1}(b,\theta) - \frac{\partial u_r}{\partial K_1}(b,\theta_m)\right] d\theta = 0 \tag{35}$$

Use of relation (32) for $u_r(b, \theta)$ and of its derivative with respect to K_1 in the integral (35) and noticing that $\theta_m = \pi/N$ leads the minimization condition in the following form:

$$\sum_{k\geq 1}\sum_{j\geq 1}\left[U_{kNy}\left(U_{jNx} + K_1 U_{jNy}\right)\right] \times S_{kj} = 0 \tag{36}$$

with S_kj given by:

$$S_{kj} = (-1)^{j+k}(\theta_m - \phi) + \frac{(-1)^k}{jN}\sin(jN\phi) + \frac{(-1)^j}{kN}\sin(kN\phi) - \frac{\sin[(j+k)N\phi]}{2(j+k)N} - \frac{\sin[(j-k)N\phi]}{2(j-k)N} \tag{37}$$

Finally, the minimization condition (36) leads K_1 as follows:

$$K_1 = -\frac{\sum_{k\geq 1}\sum_{j\geq 1} U_{kNy}.U_{jNx}.S_{kj}}{\sum_{k\geq 1}\sum_{j\geq 1} U_{kNy}.U_{jNy}.S_{kj}} \tag{38}$$

4. Comparison to finite element simulations

4.1. Hoop enrichment model

Here we consider a pellet fragment (see Fig. 1) submitted to a parabolic radial distribution of strain free stress $\hat{\epsilon}^{an}(r) = \epsilon_1^{an} + \epsilon_3^{an} r^2$ and a contact pressure P_c. The parabolic form of the stress free strain is representative of thermal strains experienced by fuel pellets (Bailly et al., 1968).

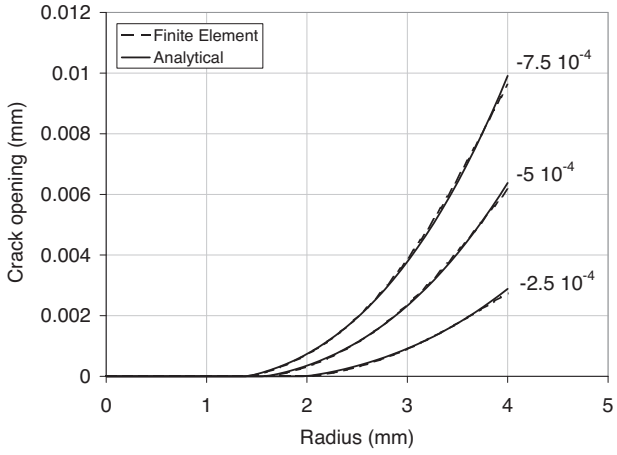

Fig. 4. Impact of the thermal strains magnitude ($\epsilon_3^{an} = -2.5 \times 10^{-4}$, -5×10^{-4} and -7.5×10^{-4} mm^{-2}) on the crack opening calculated with the finite element and analytical models.

In this particular situation, there are six unknown coefficients (α_3, β_3, A, r_0, γ, P_c). First, (α_3, β_3) are explicitly derived from the two relations in (8). Then, A is derived from relation (12). Finally the contact radius R_c and the two parameters (r_0, γ) are deduced from relations (14), (15) and (17).

This approximation of the pellet crack opening ($u_\theta(r, \theta_m)$) is now compared to 2D plane strain simulations performed with the finite element code Cast3M (Cast3M, 2011). The mesh and boundary conditions are described in Fig. 3. Unilateral contact conditions are considered on the fracture plane, i.e., $u_\theta(r, \theta_m) \leq 0$. Note that the contact radius (smallest radius where $u_\theta < 0$) is not predefined in the finite element simulations but results from the mechanical equilibrium of the fragment submitted to a parabolic distribution of strain ($\hat{\epsilon}^{an}(r)$) and to a constant external pressure (P_c).

In Fig. 4, the crack width (absolute value) along the radius of the pellet fragment is plotted for three different thermal strain magnitudes ($\epsilon_3^{an} = -2.5\,10^{-4}$, -5.10^{-4} or $-7.5\,10^{-4}$ mm^{-2}). The remaining parameters are constant ($P_c = 80$ MPa, $E = 200$ GPa, $\nu = 0.3$, $N = 12$). As expected, increasing thermal strains leads to higher tip crack openings and smaller contact radii. The agreement between the finite element solutions and the analytical estimates is excellent.

In Fig. 5, the impact of the contact pressure on the crack opening is assessed ($\epsilon_3^{an} = -5.10^{-4}$ mm^{-2}, $E = 200$ GPa, $\nu = 0.3$, $N = 12$ and $P_c = 5$ MPa or 80 MPa). Increasing the contact pressure leads to smaller crack tip openings with greater contact radii. These results illustrate the closing of pellet radial cracks when strong PCI takes place. The agreement with the finite element solutions is again excellent.

Finally, the impact of the fragment size ($N = 8$, 12 or 16) on the crack opening is illustrated in Fig. 6 ($\epsilon_3^{an} = -5.10^{-4}$ mm^2, $E = 200$ GPa, $\nu = 0.3$, $P_c = 80$ MPa). Increasing the number of fragments in the pellet obviously tends to reduce the crack tip opening but has very little impact on the contact radius. The analytical results are very close to the finite element solutions when $N = 12$ or 16. The agreement is however less good when $N = 8$. The crack tip opening is well estimated but the curvature of the curve is too pronounced and the contact radius is slightly overestimated (by

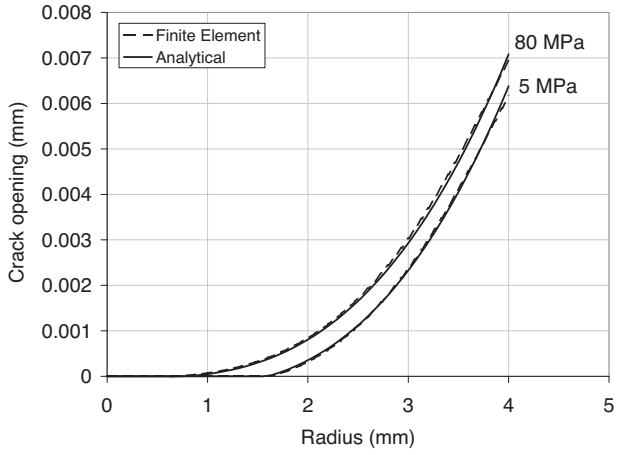

Fig. 5. Impact of the contact pressure (P_c = 5 MPa or 80 MPa) on the crack opening calculated with the finite element and analytical models.

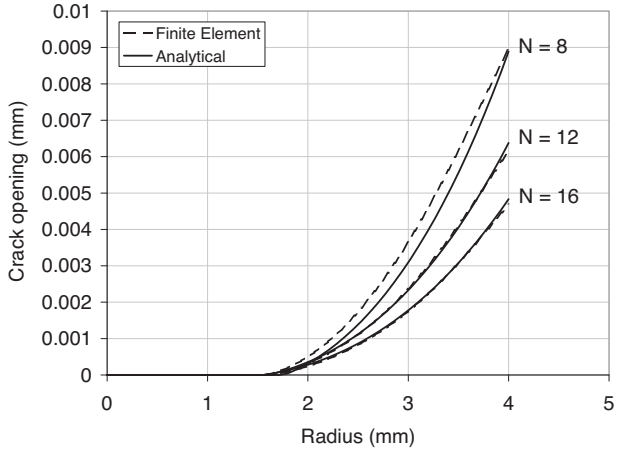

Fig. 6. Impact of the number of fragments (N = 8, 12 or 16) on the crack opening calculated with the finite element and analytical models.

10%). This result is due to the approximation used in the analytical model to comply with the boundary condition on the pellet external surface. The contact pressure is equilibrated by the average radial stress which does not ensure that the latter is constant along θ. As shown in Fig. 7, when the fragment angle θ_m is important, the

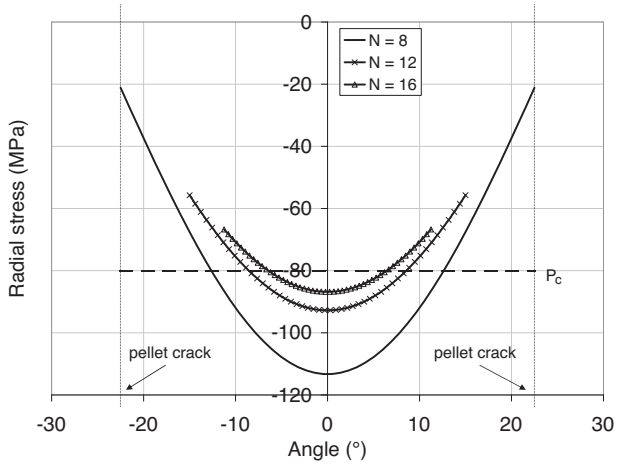

Fig. 7. Radial stresses on the pellet external surface versus angular position (zero is at the symmetry axis) as calculated by the analytical model for N = 8, 12 and 16.

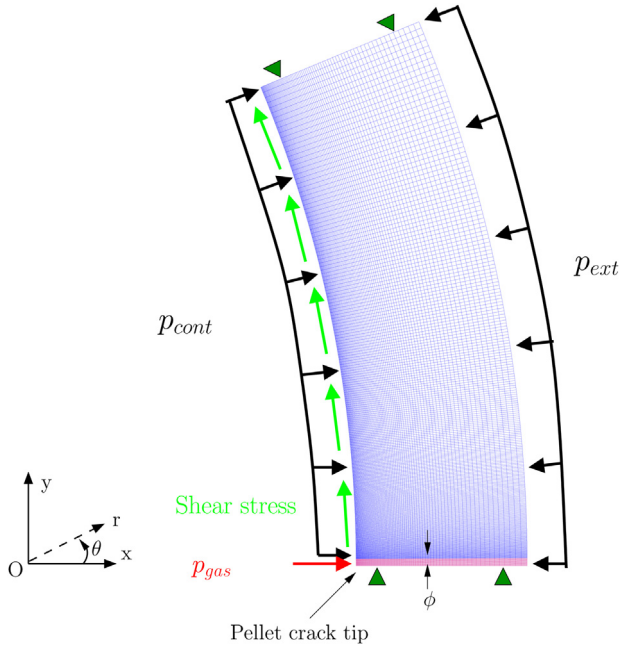

Fig. 8. Clad mesh, boundary and loading conditions in the finite element simulations with CAST3M (N = 8).

variation of the radial stress along the fragment periphery is significant ($-113 \leq \sigma_{rr} \leq -22$ MPa for N = 8 compared to $-87 \leq \sigma_{rr} \leq -67$ MPa for N = 16) and leads to the observed differences.

4.2. Stress concentration model

To assess the solution for the stress concentration problem, a two-dimensional model of the cladding with prescribed shear and radial stresses on its inner and outer walls has been built and solved with the finite element code Cast3M (Cast3M, 2011). The mesh of the cladding together with the boundary and loading conditions are given in Fig. 8. We assume here that the pellet is fragmented in N = 8 pieces and because of the symmetries, we represent only one sixteenth of the clad cylinder (θ_m = 22.5°). The mesh size in the angular and radial directions is equal to 1 μm to catch the stress/strain concentration in front of the crack tip. The cladding has standard dimensions and material characteristics for Stress-Relieved Zircaloy-4 PWR fuel rods (a = 4.741 mm, b = 4.171 mm, E = 72 GPa, ν = 0.34). The mean contact pressure on the inner wall of the cladding is $p_{cont}^{mean} = 92$ MPa, the gas pressure is p_{gas} = 11.8 MPa, the external pressure (p_{ext}) equals 15.5 MPa.

The analytical and finite element solutions are obtained as follows. First, the minimization of the angular variation of the radial displacement (Eq. (34)) leads to the optimum slope K_1 for the contact pressure distribution on the clad inner surface (a crack tip opening of ϕ = 22 μm and a friction coefficient of 0.47 are considered). The resulting linear variation of the contact pressure and shear stress are then applied in the finite element model, apart from the first 22 μm of the clad inner surface where the gas pressure is applied. The displacements and stress fields obtained from the stress concentration and finite element models are compared in Figs. 9–11. They are represented in function of the angular position. The agreement is excellent. The radial displacement of the inner clad surface is as expected nearly uniform. The tangential displacement is zero at the lower and upper boundaries of the cladding bore (θ = 0° and θ = 22.5°) and maximum near mid-angle position. Small differences appear in the hoop stress and tangential displacement distributions. They are probably due to the small differences in the

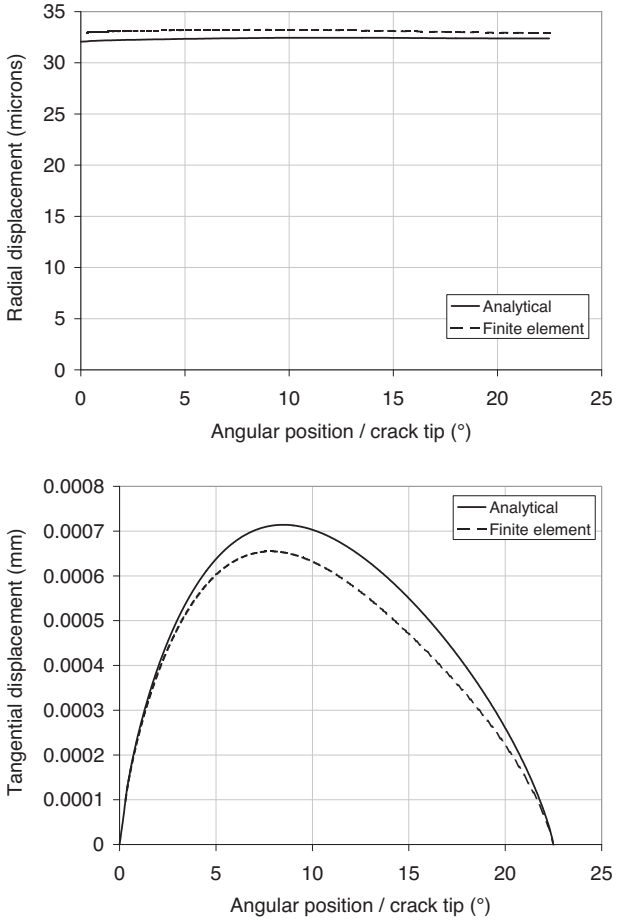

Fig. 9. Clad inner wall radial (top) and tangential (bottom) displacements as given by the analytical and finite element models.

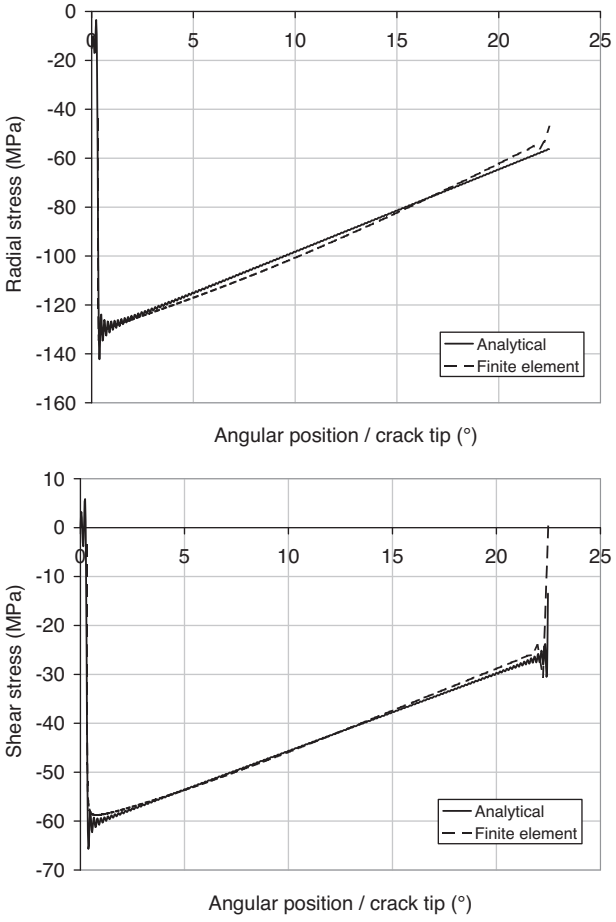

Fig. 10. Clad inner wall radial (top) and shear (bottom) stress distributions as given by the analytical and finite element models.

radial and shear stresses applied on the inner wall. Oscillations are present in the analytical curves near the two boundaries where strong variations of either the radial or shear stress take place. Near the crack tip, the radial stress variation $p_{cont} - p_{gas}$ reaches almost 120 MPa while the shear stress drops by 60 MPa. At the plane of symmetry of the fragment, the shear stress changes sign and hence leads to a 50 MPa variation. The Fourier expansion of the boundary conditions that is used in the derivation of the stresses does not ensure a perfect match of these sudden stress variations and hence leads to small differences with respect to the finite element solution. Nevertheless, the main features of the stress and displacement curves are well catched by the closed-form solution.

5. Comparison of closed-form solutions with ALCYONE

5.1. Short description of ALCYONE

ALCYONE is a multi-dimensional fuel performance code (Sercombe et al., 2009) dedicated to the modeling of the in-reactor behavior of PWR fuel rods during normal (base irradiation) and off-normal (power ramps) operating conditions. It incorporates three schemes which allow a more or less precise description of pellet cladding interaction. A reference scheme, based on a one-dimensional axi-symmetric description of the fuel element associated to a discrete axial decomposition of the fuel rod in stacked independent fuel slices, similar to the one available in many fuel performance codes (Lassmann and Blank, 1988; Baron et al., 2008; Garnier et al., 2009), is used to study the behavior of the complete fuel rod. A two-dimensional scheme which describes PCI at the mid-pellet plane of a pellet fragment is available to assess precisely stress concentration in the cladding near a pellet crack tip (Michel et al., 2008). A three-dimensional model of the complete pellet fragment and overlying cladding is also of interest when detailed studies of PCI at pellet–pellet interfaces are required. The different schemes use the Finite Element (FE) code Cast3M (Cast3M, 2011) to solve the thermo-mechanical problem and share the same physical material models at each node or integration points of the FE mesh.

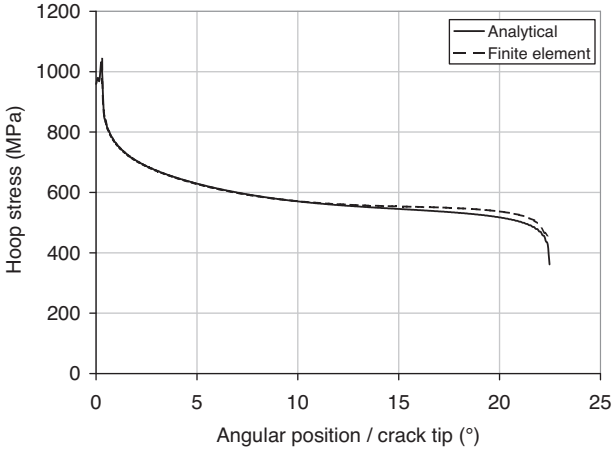

Fig. 11. Clad inner wall hoop stress distributions as given by the analytical and finite element models.

Table 1
Summary of the models used in the simulations performed with ALCYONE.

Fuel properties	
Thermal conductivity	Modified Lucuta's formulation (Lucuta et al., 1996)
Thermal expansion coefficient	Martin's formulation for UO_2 (Martin, 1988)
Elasticity coefficients	Martin's formulation for temperature dependency (Martin, 1989)
Radial power profiles	Modified version of RADAR (Palmer et al., 1992)
Clad properties	
Thermal conductivity	SRA Zy-4 temperature-dependent model (MATPRO, 1997)
Thermal expansion coefficient	SRA Zy-4 anisotropic model (Internal CEA report, 1981)
Elasticity coefficients	SRA Zy-4 isotropic model (Internal CEA report, 1981)
Inelastic clad behavior	SRA Zy-4 anisotropic formulation based on Hill's criterion (Soniak et al., 2002) Irradiation-induced creep, low-stress creep
Pellet-clad interface	
Pellet-clad gap thermal heat transfer	URGAP model (Lassmann and Hohlefeld, 1987)
Friction between pellet and cladding	Coulomb law (Cast3M, 2011)

A detailed description of the main phenomena considered in the thermo-mechanical code ALCYONE can be found in Michel et al. (2008) and Sercombe et al. (2012). Many non-linear behavior are generally considered simultaneously: creep and cracking of the pellet, clad creep and plasticity, clad-pellet friction, stress-dependent gas swelling. Since the closed-form solutions have been derived for simplified loading conditions and material behavior, only part of the phenomena are considered in the simulations presented hereafter in this paper, see Table 1. Creep and secondary cracking of the fuel pellet are neglected, i.e., linear elasticity is assumed. Thermal swelling is the only strain component considered in the calculations. The thermal conductivity of the pellet material and its elastic properties (shear modulus, Poisson's ratio) are however temperature and porosity dependent. Concerning the cladding, the dependency of its mechanical properties on temperature is taken into account.

5.2. Case study

Hereafter, only the two-dimensional scheme of ALCYONE will be used to assess the performance of the proposed closed-form solutions in realistic in-reactor conditions. The mesh, boundary and loading conditions are described in Fig. 12. We assumed here that the pellet is fragmented in $N = 8$ or 16 pieces which is

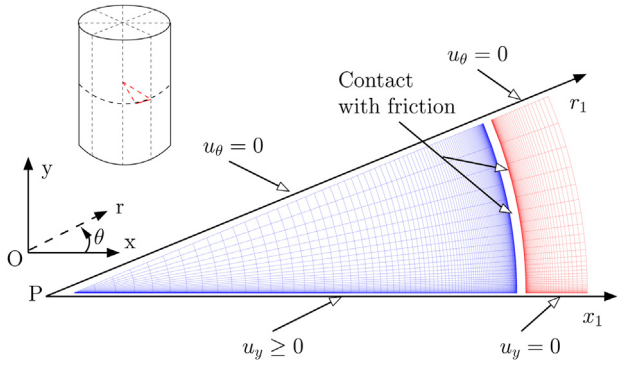

Fig. 12. Mesh and boundary conditions in ALCYONE simulations.

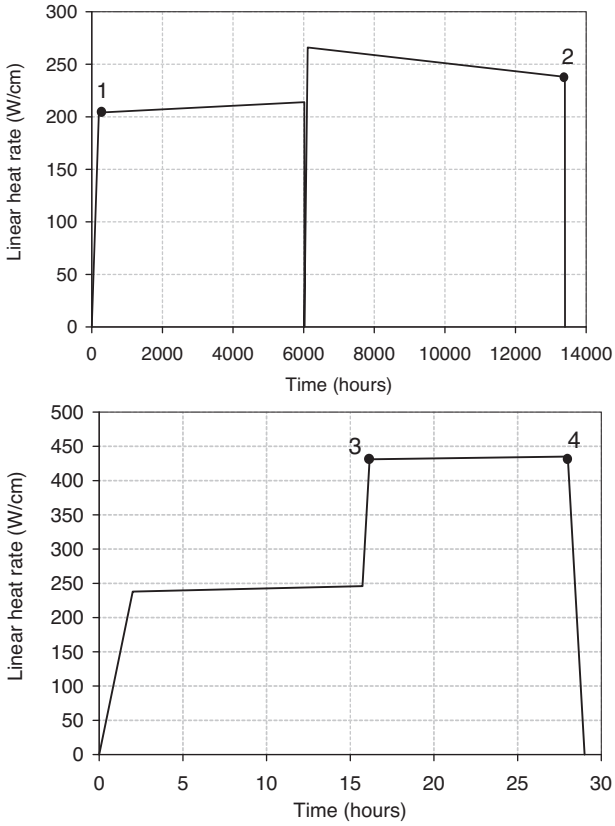

Fig. 13. Irradiation history during normal (base irradiation, top) and off-normal (power ramp, bottom) operating conditions.

consistent with the fragmentation of the pellets after base irradiation (Sercombe et al., 2012). The boundary conditions account for the geometrical symmetries of the problem and for the pellet-cladding and pellet–pellet interactions. Pellet–pellet interpenetration along the fracture plane (Px_1) is forbidden by the unilateral contact condition $u_y \geq 0$ (note that the position of the fracture plane is reversed compared to Fig. 3). The mesh size is close to 1 μm near the fracture tip. Concerning loading conditions, the gas pressure is applied to the cladding inner surface and on the pellet fragment outer surface when the gap is open. The external pressure is applied to the cladding outer surface. At the pellet-cladding interface, unilateral contact is assessed at each time step and a Coulomb model is introduced to simulate friction-slip or adherence (Sercombe et al., 2012). It must be emphasized that it is the mechanical equilibrium of the pellet fragment-cladding system which provides here the radial and shear stress distributions on the clad inner surface. Generalized plane strain conditions are considered in the calculations which slightly differ from the plane strain assumption used in the derivation of the closed-form solutions. Out-of-plane strains and stresses are thus calculated by ALCYONE and a locking condition on the axial strains is prescribed upon closure of the pellet-clad gap.

Two realistic in-reactor loading conditions are considered in the simulations. Fig. 13 gives the evolution of linear heat rate during a 2 cycle-long base irradiation and a power ramp. The four points mentioned in Fig. 13 indicate the times at which simulation results are compared to the closed-form solutions. Each of these points presents salient features: at point 1, the pellet clad gap is still open, at point 2, weak PCI occurs (small contact pressure), at point 3, strong PCI occurs (high contact pressure and shear stresses), at point 4, significant stress relaxation has taken place with sliding at the pellet-clad interface. Irradiation creep of the stress-relieved

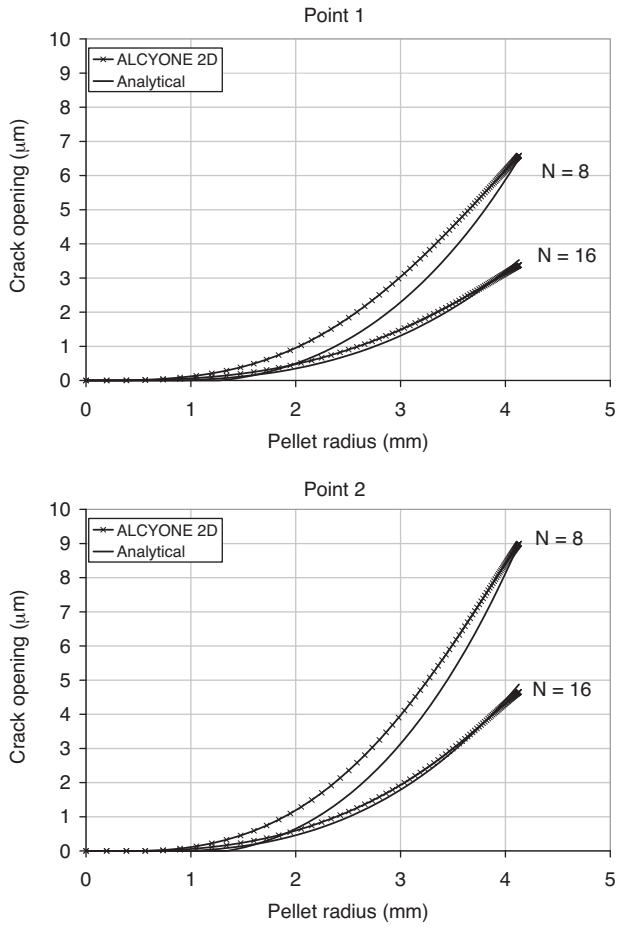

Fig. 14. Crack opening at different times during base irradiation according to the proposed analytical solution and ALCYONE.

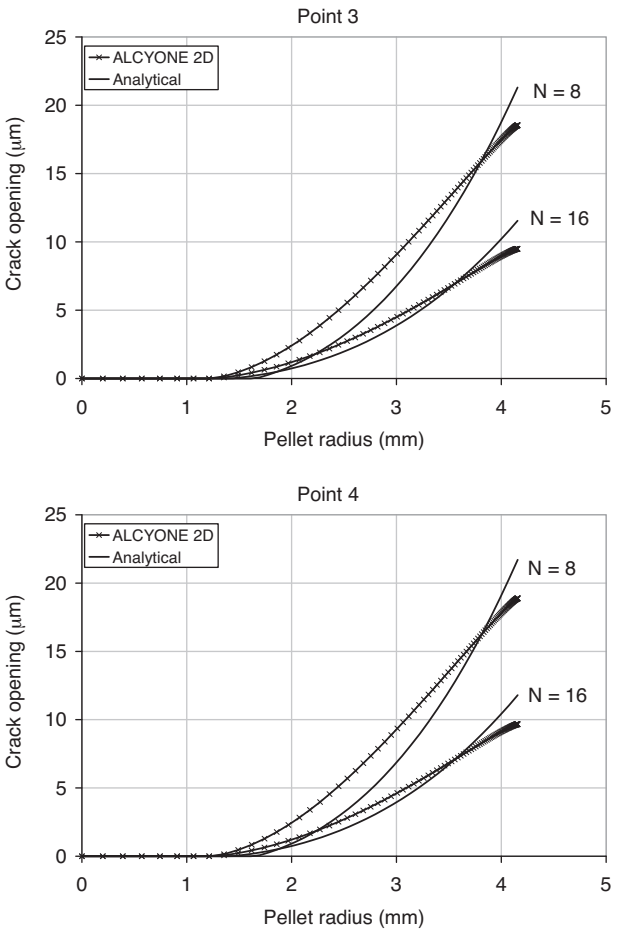

Fig. 15. Crack opening at different times during power ramping according to the proposed analytical solution and ALCYONE.

Zircaloy-4 cladding material is considered during base irradiation to allow for realistic gap closure times, see Table 1. Elastic behavior of the cladding holds during the power ramp to allow meaningful comparison with the stress concentration model.

5.3. Opening of the pellet crack

To apply the closed-form solution for the crack opening, some input data are necessary: the Poisson ratio ν and shear modulus G, the outer pellet radius R, the contact pressure P_c and the radial thermal strain distribution $\hat{\epsilon}^{an}(r)$. At each time step of interest, the first four input data are obtained from ALCYONE by averaging their variations in the angular direction. The radial thermal strain profile is deduced from the strains calculated by ALCYONE at the pellet center and periphery assuming a parabolic distribution. Note that this methodology leads to small differences in the thermal strains profile since the thermal conductivity used in the fuel code ALCYONE is temperature and porosity-dependent. The opening of the pellet crack along the pellet radius according to expression (4) and following the steps described in Section 4.1 is then estimated at different times.

The opening of the pellet crack along the pellet radius estimated at different times according to the closed-form solution are compared in Figs. 14 and 15 to those calculated by ALCYONE. Fig. 14 shows that the closed-form solution compares relatively well with ALCYONE during base irradiation. In particular, the near-tip crack opening is well reproduced when pellet-clad contact is not effective or weak (points 1 and 2). In the case of the $N = 8$ initial fragmentation, the contact radius is slightly overestimated and the curvature of the curve is also too pronounced as it was found previously. Again, if the fragment size is important, the approximation of the radial stress distribution on the outer surface of the fragment is rather crude and at the origin of the differences.

As shown in Fig. 15, during the power ramp, when strong pellet-clad contact occurs (points 3 and 4), the near-tip crack opening is overestimated by 10–15% independently of the fragmentation ($N = 8$ or 16). The shape of the crack opening-radius curves obtained with ALCYONE is far from being characterized by a r^3 dependency as would be expected from the analytical solution. The strong angular variation of the contact pressure given by ALCYONE (see Fig. 17) where the contact pressure is markedly peaked in front of the crack is at the origin of the quasi-linear evolution of the crack width with the radius. Friction at the pellet-clad interface also tends to hinder the crack opening and explains the shape of the curve near the crack tip. In spite of these local differences, the closed-form solution leads a reasonable estimation of the contact radius during the power ramp, in particular when $N = 16$. On average, the impact of the contact pressure on the crack opening is thus correctly assessed.

5.4. Stress concentration in the cladding

The displacements and stresses are now compared at the top of the ramp (point 3) since this time is generally considered as the critical time with respect to clad failure. Average values for the internal and external radii (b and a) of the cladding, for the shear modulus (G) and Poisson ratio (ν) of the cladding and for the contact pressure

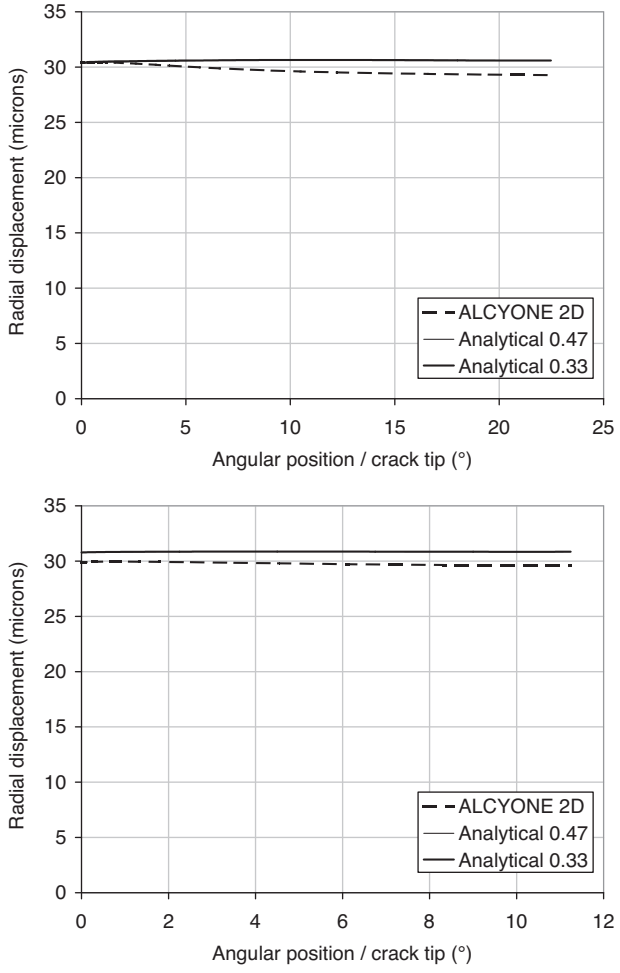

Fig. 16. Clad inner wall radial displacements as given by ALCYONE and the analytical models (top: $N = 8$, bottom: $N = 16$).

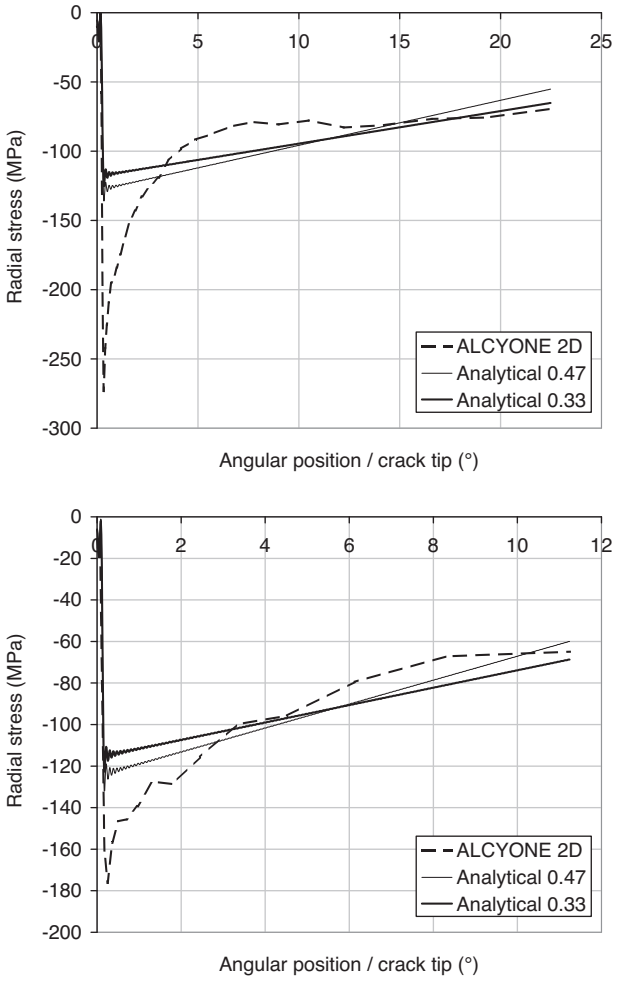

Fig. 17. Clad inner wall radial stress distribution as given by ALCYONE and the analytical models (top: $N = 8$, bottom: $N = 16$).

p_{cont}^{mean} are deduced from ALCYONE simulations and used as input data in the stress concentration model. The friction coefficient μ, the gas and coolant pressures (p_{gas} and p_{ext}) are directly injected in the closed-form equations. The crack width ϕ is computed from the pellet displacement field (4) according to the following relation:

$$2\phi R = 2|u_\theta(R, \theta_m)| \tag{39}$$

It has been checked that the 15% error oberved in the estimation of the crack width had no impact on the stresses determined by the stress concentration model. The test of Section 4.2 has been recalculated with a crack opening of 18 μm instead of 22 μm and lead to a left shift of the stress–angular position curves with absolutely no change in the peak stresses.

The two main assumptions behind the derivation of the closed-form solution are first that the angular variation of the contact pressure is linear and second that the radial displacement of the inner clad surface is almost uniform. As illustrated in Fig. 16 (top), results obtained with ALCYONE at point 3 (dashed line) confirm the constancy of the radial displacement. However, the assumption of a linear angular variation for the radial stresses does not seem to match perfectly the curve obtained with ALCYONE, see Fig. 17 (top). A pronounced radial stress peak exists in the vicinity of the crack tip. The overall shape of the curve is thus closer to an exponential function of the angular position as proposed by Gittus (1972) in his pioneering work on the subject.

Obviously, as for the crack opening, the angular variation of the contact pressure must depend on the size of the pellet fragment. In fact, ALCYONE simulations with a pellet divided in $N = 16$ pieces instead of $N = 8$ show that in this case the assumption of a linear angular variation in contact pressure is more reasonable, see Fig. 17 (bottom). The evenness of the radial displacement of the inner clad surface is also confirmed, see Fig. 16 (bottom).

The hoop stresses at the top of the ramp (point 3) are now compared in Fig. 18 for the $N = 8$ and $N = 16$ cases. ALCYONE results are plotted with dashed lines. The analytical curves obtained with a friction coefficient of 0.47 are plotted with thin full lines. The hoop stress variation along the clad inner wall is correctly approximated by the closed-form solution with however some marked differences near the crack tip. First, the maximum hoop stress is overestimated: for $N = 8$, ALCYONE gives a maximum of 920 MPa compared to 1000 MPa for the analytical solution, for $N = 16$, ALCYONE gives 905 MPa compared to 985 MPa). Second, the radial stress distribution with a pronounced peak near the crack tip leads to some local bending of the cladding with a reduction in the hoop stresses on the inner wall. The perturbation decreases with the intensity of the radial stress peak and hence with the number of fragments.

The magnitude of hoop stresses in front of a pellet crack depends mainly on the magnitude of the shear stresses applied at the pellet clad interface (Michel et al., 2008). It is important to recall that the shear stresses in the closed-form solution are simply given by

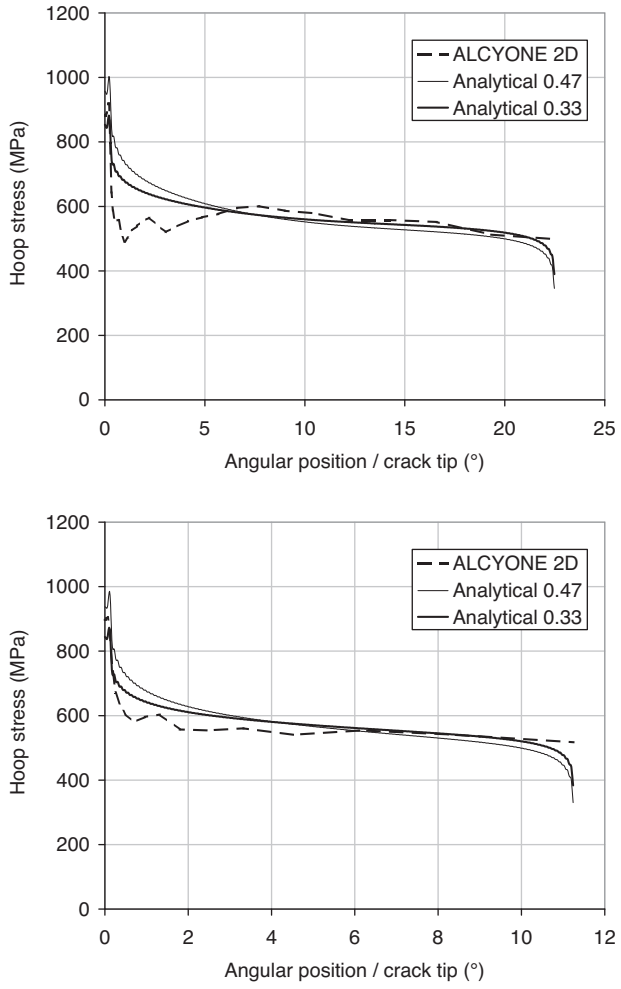

Fig. 18. Clad inner wall hoop stress distribution as given by ALCYONE and the analytical models (top: $N = 8$, bottom: $N = 16$).

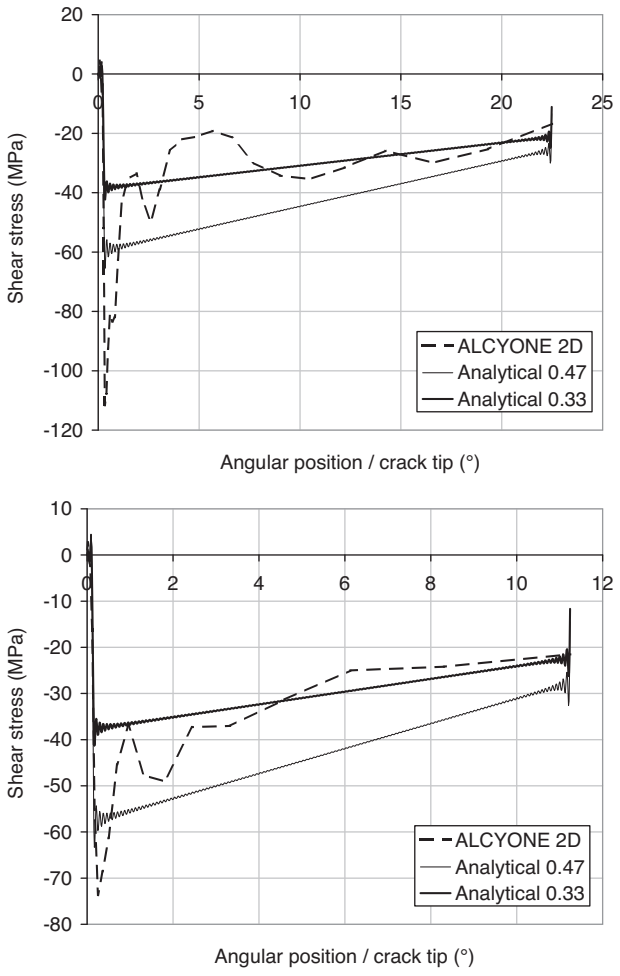

Fig. 19. Clad inner wall shear stress distribution as given by ALCYONE and the analytical models (top: $N = 8$, bottom: $N = 16$).

the radial stress profile and the constant friction coefficient (0.47) under the assumption that sliding occurs everywhere at the pellet fragment clad interface. As shown by the comparison of the shear stresses given in Fig. 19, ALCYONE simulations (dashed line) tend to give much lower shear stresses than the stress concentration model (thin full line, 'Analytical 0.47'). This indicates that sliding at the pellet-clad interface is not effective everywhere, in particular in the near-tip region. The ratio of the shear stresses to the radial stresses shows that only a small portion of the inner clad wall ($0.3 < \theta < 0.8^\circ$) reaches a value greater than 0.4.

To check that the differences in shear stress magnitude are at the origin of part of the overestimation of the hoop stress concentration, the analytical solution has been recalculated with a friction coefficient more representative of the stress profiles calculated by ALCYONE. The ratio of the average shear stress to the average radial stress led to a friction coefficient equal to 0.33 irrespective of the number of fragments N. Note that this value does not reflect real friction conditions. It only represents better the shear stress distribution calculated by ALCYONE. With this value, the closed-form solution led to a better estimation of the maximum hoop stresses (882 MPa for $N = 8$, 873 MPa for $N = 16$), compare the dashed lines to the thick solid lines in Fig. 18. The closer matching of the shear stress distributions as given by ALCYONE and the analytical model can now be seen in Fig. 19. Note that the change in the friction coefficient brought also small changes in the slopes of the contact pressure–angular position curves, see the thin and thick full lines in Fig. 17.

6. Conclusion

In this paper, closed-formed solutions concerning pellet cladding interaction have been proposed and compared to 2D finite elements simulations. The first solution gives the opening of a radial crack in a pellet fragment subjected to a radial thermal gradient and loaded by a uniform external pressure. The second solution describes the stress state in a cylindrical cladding loaded by a pellet fragment and catches the stress concentration in front of an opening pellet radial crack. Analytical estimates were found in good agreement with finite element results.

The usefulness of the solutions was checked by comparing their response at different times during base irradiation and power ramp irradiation histories with that of the 2D scheme of the fuel performance code ALCYONE. Overall, the closed-form solutions were able to give reasonable estimates of the radial crack opening of the pellet fragment and of the hoop stress distribution in the cladding during typical in-reactor loading sequences.

These models are of interest to enhance the representativity of multi-dimensional fuel codes and or to confirm the robustness of standard fuel performance codes which are usually based on a one-dimensional description of PCI. With the proposed approach, a three-dimensional based PCI failure criterion such as the one proposed by Michel et al. (2008) could eventually be used by post-processing the calculation results of a standard one-dimensional code.

These models could also be used to develop or interpret complex experiments. The mandrel tests, such as the one developed in reference (Anghel et al., 2010) for I-SCC studies is a good example of a complex experiment where the need for models capable of capturing the stress and strain localization due to fragments would be useful. Preliminary sensitivity analyses could give some clues on the importance of pellet fragment size, crack opening, friction at the fragment-clad interface.

Acknowledgements

The authors would like to thank the students that worked successively on the subject for their master thesis, namely Sébastien Muller, Mathieu Turban, Ludovic Giusti, Julien Graffard and Jean-Marc Bot. The authors acknowledge EDF and AREVA for their financial support to this research.

References

Anghel, C., Alvarez Holston, A.M., Lysell, G., Karlsson, J., Jakobsson, J., 2010]. Experimental and finite element modeling parameter study for iodine induced stress corrosion cracking of irradiated cladding. In: TopFuel2010 Conference, Orlando, September, pp. 218–228.

Bailly, H., Ménessier, D., Prunier, C., 1968. Le combustibles nucléaire des réacteurs à eau sous pression et des réacteurs à neutrons rapides, Eyrolles Eds., Paris, France.

Baron, D., Thevenin, P., Largenton, R., Masson, R., 2008]. CYRANO3 the EDF fuel code performance especially designed for engineering applications. In: Proc. of the Water Reactor Fuel Performance Meeting, Seoul, Corea, Paper 8032.

Brochard, J., Bentejac, F., Hourdequin, N., Seror, S., Verdeau, C., Fandeur, O., Lansiart, S., Verpeaux, P., 2001]. Modelling of pellet cladding interaction in PWR fuel. In: Proceedings of the SMIRT 16 Conference, Washington DC, USA.

Cast3M, 2011. http://www-cast3m.cea.fr/cast3m/index.jsp

Cox, B., 1990]. Pellet-clad interaction (PCI) failures of zirconium alloy fuel cladding—a review. J. Nucl. Mater. 172, 249–292.

Garnier, C., Sontheimer, F., Mailhé, P., Landskron, H., Deuble, D., Arimescu, V.I., Bellanger, Ph., 2009]. Validation of advanced fuel performance COPERNIC3 code on AREVA global database up to 100 GWd/thm. In: Proceedings of Top Fuel Conference, Paris, France.

Gittus, J.H., 1972]. Theoretical analysis of the strains produced in nuclear fuel cladding tubes by the expansion of cracked cylindrical fuel pellets. Nucl. Eng. Des. 18, 69–82.

Jackson, P.A., 1987]. The effect of pellet wheatsheaf growth during power ramps on cladding stress concentration. Nucl. Eng. Des. 101, 225–232.

Lassmann, K., Hohlefeld, F., 1987]. The revised URGAP model to describe the gap conductance between fuel and cladding. Nucl. Eng. Des. 103, 215–221.

Lassmann, K., Blank, H., 1988]. Modelling of fuel rod behaviour and recent advances of the TRANSURANUS Code. Nucl. Eng. Des. 106, 291–313.

Levy, S., Wilkinson, J.P.D., 1974]. Three-dimensional study of nuclear fuel rod behavior during startup. Nucl. Eng. Des. 29, 157–166.

Lucuta, P.G., Matzke, H.S., Hastings, I.J., 1996]. A pragmatic approach to modelling thermal conductivity of irradiated UO_2 fuel: review and recommendations. J. Nucl. Mater. 232, 166–180.

Marchal, N., Campos, C., Garnier, C., 2009]. Finite element simulation of pellet-cladding interaction (PCI) in nuclear fuel rods. Comp. Mater. Sci 45, 821–826.

Martin, D.G., 1988]. The thermal expansion of solid UO_2 and (U, Pu) mixed oxides—a review and recommendations. J. Nucl. Mater. 152, 94–101.

Martin, D.G., 1989. High Temperature–High Pressures. 21, 13–24.

MATPRO, 1997. A library of Material Properties for Light-Water-Reactor Accident Analysis. NUREG/CR-6150, Vol 4, Rev1.

Michel, B., Sercombe, J., Thouvenin, G., 2008]. A new phenomenological criterion for pellet cladding interaction rupture. Nucl. Eng. Des. 238, 1612–1628.

Muskhelishvili, N.I., 1963]. Some Basic Problems of the Mathematical Theory of Elasticity, 4th Ed. P. Noordhoff, Groningen, The Netherlands.

Nakatsuka, M., 1981]. Theoretical and experimental analyses of cladding strain produced by expansion of cracked fuel pellets. Nucl. Eng. Des. 65, 197–204.

Palmer, I.M., Hesketh, K.W., Jackson, P.A., 1992]. A model for predicting the radial power profile in a fuel pin. In. In: IAEA Specialists' meeting on Water Reactor Fuel Element Performance, pp. 321–335.

Ranjan, G.V., Smith, E., 1980]. Determination of stress within zircaloy cladding due to pellet cladding interaction. Nucl. Eng. Des. 56, 263–272.

Retel, V., Trivaudey, F., Boubakar, M.L., Perreux, D., Thevenin, Ph., 2004]. Comparative effects of structural and material parameters variability on Pellet-Cladding Interaction in a PWR fuel rod. Nucl. Eng. Des. 228, 35–46.

Roberts, G., 1978]. The concentration of stress in cladding produced by the expansion of cracked fuel pellets. Nucl. Eng. Des. 47, 257–266.

Sercombe, J., Michel, B., Thouvenin, G., Petitprez, B., Chatelet, R., Leboulch, D., Nonon, C., 2009]. Multi-dimensional modeling of PCMI during base irradiation and ramp testing with ALCYONE V1. 1. In: Proceedings of Top Fuel Conference, Paris, France.

Sercombe, J., Aubrun, I., Nonon, C., 2012]. Power ramped cladding stresses and strains in 3D simulations with burnup-dependent pellet-clad friction. Nucl. Eng. Des. 242, 164–181.

Soniak, A., L'hullier, N., Mardon, J.-P., Rebeyrolle, V., Bouffioux, P., Bernaudat, C., 2002]. Irradiation creep behavior of Zr-base alloys. In: Zirconium in the Nuclear Industry: 13th International Symposium, ASTM STP 1423, Annecy, France, pp. 837–862.

Yaung, J.Y., Okrent, D., Wazzan, A.R., 1985]. A simple computer model of pellet/cladding interaction including stress corrosion cracking. Nucl. Tech. 71, 644–650.